Journal of Applied Physics

RESEARCH ARTICLE | NOVEMBER 10 2023

a-C/GeTe superlattices: Effect of interfacial impedance adaptation modeling on the thermal properties

Paul Desmarchelier ; Valentina M. Giordano ; Jean-Yves Raty ; Konstantinos Termentzidis

Check for updates

J. Appl. Phys. 134, 185105 (2023)
https://doi.org/10.1063/5.0167166

View Online
Export Citation
CrossMark

19 December 2023 12:28:58

AIP Publishing

Journal of Applied Physics ARTICLE pubs.aip.org/aip/jap

a-C/GeTe superlattices: Effect of interfacial impedance adaptation modeling on the thermal properties

Cite as: J. Appl. Phys. **134**, 185105 (2023); doi: 10.1063/5.0167166
Submitted: 10 July 2023 · Accepted: 23 October 2023 ·
Published Online: 10 November 2023

View Online Export Citation CrossMark

Paul Desmarchelier,[1,2,a)] Valentina M. Giordano,[3] Jean-Yves Raty,[4] and Konstantinos Termentzidis[1]

AFFILIATIONS

[1]Univ. Lyon, CNRS, INSA Lyon, CETHIL, UMR5008, 69621 Villeurbanne, France
[2]DMSE, Johns Hopkins University, Baltimore, Maryland 21218, USA
[3]Institut Lumiere Matière, UMR 5306 Universite Lyon 1-CNRS, F-69622 Villeurbanne Cedex, France
[4]Condensed Matter Simulation, CESAM, Universite de Liege, 19 Allee du 6 Aout, Sart-Tilman 4000, Belgium

[a)]**Author to whom correspondence should be addressed:** paul.desma@gmail.com

ABSTRACT

Recently, nanostructuration has been proposed to improve the performance of phase change memories. This is the case of superlattices composed of amorphous carbon and crystalline germanium telluride, which we have investigated by molecular dynamics. For this, a modified Stillinger–Weber potential is adapted to reproduce their stiffness contrast/impedance ratio. In order to study the effect of the interface interaction, two sets of parameters are used to model the interfaces with different interactions between the two materials using the properties of the softer material or the average properties between the two creating an adaptation of impedance across the layers. The effects of interface roughness and carbon diffusion at grain boundaries are studied. Using equilibrium molecular dynamics as well as the propagation of wavepackets, we show first that without impedance adaptation, the anisotropy is high, and the roughness has a marked impact on the properties. However, the introduction of impedance adaptation destroys those effects on the thermal conductivity. Finally, we show that the periodic texturing of the interface increases the transmission of in-plane transverse phonons.

Published under an exclusive license by AIP Publishing. https://doi.org/10.1063/5.0167166

19 December 2023 12:28:58

I. INTRODUCTION

One of the current societal challenges is the discovery of new green energy sources and the reduction of energy consumption. In this context, it is important to develop new strategies for improving the efficiency of information processing electronics and of waste heat recovery. Such strategies are usually concerned with the development of materials with low thermal conductivity. Indeed, this is the need for increasing thermal confinement in microelectronic applications, such as, phase change memories.[1] Lower thermal conductivity also improves the thermoelectric conversion of heat into electricity.[2] Both require materials with low thermal conductivity. One of the strategies to reduce the thermal conductivity is to use a nanostructuration and, in particular, a high interface density.

Superlattices, in which thin layers of different materials are alternated, have lower thermal conductivity than the constitutive material due to their high density of interfaces.[3] This has been interpreted as due to two possible mechanisms: on one side, the incoherent scattering of phonons at the interfaces (Kapitza resistance)[4] on the other, the coherent effect of a periodic nanostructure, which modifies the phonon dispersion due to the definition of a new Brillouin zone. This leads to branch folding, a decrease of the group velocity, a change of phonon density of states, and a possible opening of bandgaps. This mechanism requires that phonon scattering at the surface is specular, which requires very small interface roughness. As such, interface roughness plays a role in determining thermal transport properties as well, and a rough interface will increase the cross-plane and decrease the in-plane thermal conductivity.[5–7] Another condition for specular reflection is a sharp impedance contrast between the two layers,[8] i.e., the contrast in group velocities due to the mass/stiffness mismatch, preventing the transmission of phonons across the interface.

Published under an exclusive license by AIP Publishing

The structural properties of an interface and, thus, its conductance are strongly determined by the fabrication process. For instance, epitaxially grown superlattices have an atomically smooth surface where coherence effects matter.[9] In such superlattices, the very thin layers allow the coherent propagation of phonons across the interface, and this competes with the reduction of conductance due to multiplication of interfaces, leading to a minimum of thermal conductivity as a function of the period.[10] Crystalline–amorphous superlattices allow taking advantage of both the high interface density and the low thermal conductivity of amorphous materials, notably in silicon/silica superlattices.[11] Indeed, the amorphous/crystal interface prevents the transmission of high-frequency phonons[12] and has high thermal resistance.[13] These interfaces exhibit high thermal conductivity anisotropy, the cross-plane thermal conductivity being notably lower than the in-plane one.[14] Moreover, interlayer diffusion of species reduces the anisotropy but also possibly disrupts the propagation of coherent phonons.[15]

This work focuses on model superlattices constituted by alternating layers of crystalline GeTe and amorphous carbon, which have been recently proposed for phase change memory applications.[16,17] Indeed, GeTe is a phase change material with a strong contrast of electric and optical properties between the amorphous and crystalline phase, which can be used to code information in memory applications.[18] Moreover, the metavalent bonding, distinct from covalent, metallic, or ionic bonding, gives it a series of properties, which make it interesting for thermoelectric applications as well.[19–21] The proposed superlattices have been found to reduce the programming currents in memory devices, suggesting a strong reduction of thermal conductivity with respect to pure GeTe thin films. The aim of this work is to model thermal transport and phonon propagation in such superlattices and understand the effect of interface quality using molecular dynamics. GeTe, due to its Peierls distortion (alternating of long and short bonds), can be challenging to model in classical MD.[20] Simulations have nevertheless been attempted with machine learning potentials.[22] Similarly, amorphous carbon (a-C) has a complex structure that depends on the density[23] and the two types of hybridization (sp2 or sp3) so that the use of conventional potentials is difficult.[24]

To circumvent these issues in the present study, a simplified model of carbon and GeTe superlattices using a Stillinger–Weber (SW) potential is used.[25] Although the topology of both species will be modified, this approach allows isolating the effect of the masses and elastic mismatch on the acoustic properties of a-C and GeTe and their interface. Studying the effect of a mass mismatch is quite common; for instance, Si/Ge superlattices have been modeled by modifying the atomic mass only while keeping the same interaction potential.[5,26,27] Here, we will combine it with an *ad hoc* modification of the interaction potential in a similar fashion as in a previous paper.[28] In this case, the dynamic interaction between the two species also has to be determined, as well as the intraspecies interaction.[29] This gives the opportunity to study both the effect of interface roughness but also of the interspecies interaction. In the following, the modeling strategy is first described, and then, two approaches to model the interaction between the layers are analyzed.

II. METHODOLOGY

A. Configuration modeling

The first step of the creation of the samples is to generate an amorphous bulk configuration. This starts with an initial crystalline block of $10 \times 10 \times 2\,\mathrm{nm}^3$, which is brought from 30 to 3500 K in 50 ps at constant volume and then annealed at this temperature for 100 ps. After this, it is quenched to 10 K at a rate of $1 \times 10^{12}\,\mathrm{K\,s^{-1}}$. This melt-quench procedure is performed using the Tersoff potential, with the mass determined in Sec. II B.[30] Then, following the procedure of Fusco *et al.*,[31] the potential is switched to the SW potential described in Sec. II B and the system is annealed at 100 K for 50 ps. The time step used for all of these simulation steps is of 0.5 fs.

To match the undergoing experimental study,[16,17] the superlattice is composed of an alternation of a 4 nm layer of GeTe and a 1 nm layer of a-C. The simulation cell only contains two periods, but periodic boundary conditions are used in all the directions to model an infinite superlattice (see Fig. 1). The two layers of a-C in the nanocomposite are taken on independent slices of the amorphous sample. The first configuration is simply composed of slices of GeTe and a-C with atomically smooth interfaces [see Fig. 1(a)].

Then, some interface roughness is introduced with one perturbation for each 10 nm wide simulation cell to reproduce experimental observations of the roughness width. To keep a maximum number of parameters constant during the simulations, the number of atoms of GeTe and C are fixed across all simulations, unless otherwise mentioned. This is done by keeping the thickness constant, the roughness being created by a simple deformation of the a-C layers, as can be seen in Fig. 1(b). For simplicity, a Gaussian shape is chosen. The height is first chosen as 1 nm and the RMS width is set to 1.5 nm, creating periodic roughness shown in Fig. 1(b). Then, some randomness is introduced by varying the height, RMS, and direction in which it protrudes between up or down. The height is sampled between 0.5 and 1.5 nm and the RMS width between 1 and 1.8 nm. Each parameter is chosen randomly out of a uniform distribution. Seven different configurations have been created, each with a different set of parameters, one of them being displayed in Fig. 1(c). The others can be seen in Fig. 15 of Appendix B 2. To study the effect of the a-C layer thickness, we double it for one of the samples [see Fig. 1(d)]. To reproduce the diffusion of carbon in GeTe grain boundaries, a configuration where a third of the GeTe atoms are randomly substituted by carbon atoms in a 4 Å thick slice in the center, at 5 nm of the box boundary, is created. This results in configuration (e) in Fig. 1. Again, here, seven configurations have been created, each with a different height, an RMS width, and a direction of protrusion. These last configurations are the only ones with a different number of C and GeTe atoms.

Up to this point, all GeTe layers share the same crystalline orientations, with x and y aligned with the ⟨100⟩ directions. To study the effect of a difference of orientation between layers, a second orientation has been introduced: x aligned with ⟨111⟩, y aligned with $\langle 1\bar{1}0\rangle$, and z aligned with $\langle 11\bar{2}\rangle$. The GeTe layers with different orientations are alternated, and this is combined with random roughness. This results in the configuration in Fig. 1(f). Again, seven iterations of this configuration with alternating orientations have been created, each with a different RMS width, height, and

19 December 2023 12:28:58

Published under an exclusive license by AIP Publishing

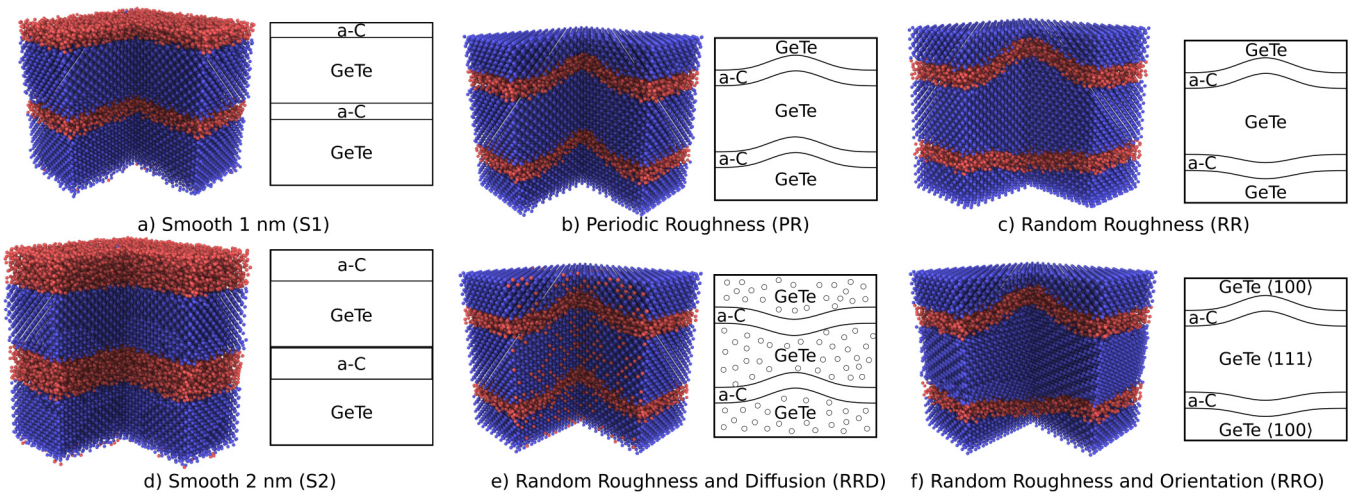

FIG. 1. Different nanocomposites studied with atomic visualization and a 2D scheme: (a) smooth 1 nm (S1), (b) periodic roughness (PR), (c) random roughness (RR), (d) smooth 2 nn (S2), (e) random roughness and diffusion (RRD), and (f) random roughness and orientation (RRO).

direction of protrusion (see Fig. 15). The configurations are created using a copy–paste method of the layer shape in the crystal and amorphous. They are relaxed with the same procedure as in Tlili *et al.*[28] The different configurations are summarized in Table I. This creates a very sharp interface, which corresponds to experimental observation.[17]

B. Interatomic potentials

The potential used is a modified Stillinger–Weber potential,[32] which has been shown to reproduce nicely the properties of silicon crystalline–amorphous nanocomposites.[13,33,34] It is modified to approximate the properties of a-C and GeTe, in particular, the acoustic impedance of the materials and the impedance mismatch between them. The impedance is defined here as $z_0 = v\rho$, with being v the group velocity and ρ being the mass density. The idea is to modify both the density and group velocity to match those of a-C and GeTe.

The GeTe is modeled, as a simplification, by a cubic diamond structure with a single atom species rather than reproducing the structure of GeTe. To modify the impedance while using the real masses (as opposed to tuning the mass only[5]), the group velocity is tuned by modifying the rigidity modulii [using the elastic theory approximation as a first approach $v \approx (K + 4/3G)/\rho$, with K being the bulk modulus and G being the shear modulus. This is done via the modifications of the pre-factor of the two and three-body components of the potentials, A_{ij} and λ_{ijk} highlighted in bold in the equations below:

$$u_2(r_{ij}) = \mathbf{A_{ij}}\epsilon_{ij}\left(B_{ij}\left(\frac{\sigma_{ij}}{r_{ij}}\right)^{p_{ij}} - 1\right)\exp\left(\frac{\sigma_{ij}}{r_{ij} - a_{ij}\sigma_{ij}}\right), \quad (1)$$

$$u_3(r_{ij}, r_{ik}, \theta_{ijk}) = \boldsymbol{\lambda_{ijk}}\epsilon_{ijk}(\cos\theta_{ijk} - \cos\theta^0)^2 \times \exp\left(\frac{\gamma_{ij}\sigma_{ij}}{r_{ij} - a_{ij}\sigma_{ij}}\right)\exp\left(\frac{\gamma_{ik}\sigma_{ij}}{r_{ik} - a_{ik}\sigma_{ik}}\right), \quad (2)$$

with B, ϵ, σ, a, θ^0, γ, and p a set of parameters fitted to reproduce the properties of Si, especially the directionality of the covalent bonding. The original values and their description can be found in the original paper of Stillinger and Weber.[25]

The mass is simply modified to reproduce the density of a-C and GeTe. Since the angles and interatomic distances are not modified, the target densities can be obtained by applying a proportionality coefficient to the atomic mass of silicon. This holds for both crystalline and amorphous phases because the melt-quench procedure used conserves the volume (see Sec. II A). This gives for a a-C of density 2.5 g/cm^3 $m^*_{a-C} = m_{c-Si}\rho_{a-C}/\rho_{a-Si} = 30.51$ g mol an average value for a-C[35] and for a GeTe of density 5.9 g/cm^3[36] $m^*_{GeTe} = m_{c-Si}\rho_{GeTe}/\rho_{c-Si} = 72.17$ g mol.

The properties of GeTe have been reproduced by modifying the prefactor in the two-body interaction $\mathbf{A_{ij}}$. It has a direct effect on the bulk modulus, as can be seen in Table II. As the elastic properties of the crystal can be quickly estimated via the explicit method,[37] a few trials are enough to find the *ad hoc* value reproducing the elastic modulii of α GeTe obtained via DFT.[38]

The bulk modulus of a-C is around 250 GPa for an a-C of density 2.5 g/cm^3.[39] To obtain this value for an amorphous sample prepared using the SW interatomic potential, the results of Fusco *et al.*[31] giving the bulk modulus as a function of the three body prefactors have been used to extrapolate the value of λ in our case. We have used a linear model and chosen a value of 150.

C. Interactions at the interface

The interactions between a-C and GeTe remain to be defined, and two approaches are considered here (see Table III). The first one is simply to use the GeTe–GeTe interaction for C–GeTe interaction; as a consequence, there is no adaptation of impedance between the a-C and GeTe layers. The second one is to use the average value between C–C and GeTe–GeTe interactions. Neither of these options is an accurate representation of the real interaction,

19 December 2023 12:28:58

Published under an exclusive license by AIP Publishing

TABLE I. Summary of the characteristics of the different configurations displayed in Fig. 1.

	a-C Thickness	Roughness		Interdiffusion	Orientation change
		Periodic	Random		
S1	1	No	No	No	No
PR	1	Yes	No	No	No
RR	1	No	Yes	No	No
S2	2	No	No	No	No
RRD	1	No	Yes	Yes	No
RRO	1	No	Yes	No	Yes

but they allow a study of two different types of interface, a first one with a sudden transition from a stiff to a soft material (no impedance adaptation) and another using a smoother transition, which is an adaptation of impedance at the interface. Something that is overlooked when modifying only the mass because it does not allow impedance adaptation.[5,26,27]

III. PROPERTIES OF THE NANOCOMPOSITES WITHOUT IMPEDANCE ADAPTATION AT THE INTERFACE

In this section, we focus on the case without impedance adaptation at the interface. To limit the complexity of the study, it will be restricted to the smooth, the periodic roughness, and the random roughness configurations. First, the thermal conductivity computed using the equilibrium molecular dynamics method (see Appendix B 1 for details) is displayed in Fig. 2. As usual in superlattices, the cross-plane and in-plane directions are compared.

A first observation is that the thermal conductivity is decreased by the nanostructuration, in particular, in the cross-plane direction, which drops below the value observed for GeTe and more importantly a-C (see Appendix A). This decrease is similar to what was already observed for a a-Si/c-Si superlattice[13] for both in-plane (κ_{IP}) and cross-plane (κ_{CP}) directions. The high impedance mismatch and the smooth interfaces most probably cause κ_{CP} being lower than κ_{a-C}. As a result, the anisotropy (κ_{IP}/κ_{CP}) is 50, which is an order of magnitude higher than for crystalline–amorphous SL without an acoustic mismatch, as will be shown in Sec. IV. This would be a typical example where the acoustic mismatch model would be suited to describe the system as the impedance mismatch is high and the interfaces are smooth. This leads to low thermal conductance thanks to stronger back scattering.[40] The roughness decreases the anisotropy by both increasing κ_{CP} and decreasing κ_{IP}. These effects have been documented before.[5,6] The random roughness seems to further increase κ_{CP} and decrease κ_{IP}. The decrease in anisotropy due to the roughness can be understood in terms of major scattering from a rough interface due to the increased specific surface and the reduced specularity. As a consequence, the diffusive mismatch model is appropriate, which is consistent with an increase of thermal conductivity with respect to the smooth surface for an interface with a strong impedance mismatch.[41] As we will see, the effect of the a-C/GeTe interface is confirmed by the results with impedance adaptation thanks to a more gradual interaction between a-C and GeTe (see Fig. 6).

TABLE II. Elastic properties of bulk GeTe as a function of the parameter A_{ij} as well as reference values from Shaltaf *et al.*[38] Boldface denotes the final value chosen for the parameter and corresponding elastic properties.

A_{ij}	K (GPa)	v	G (GPa)
7.05	101	0.34	56
6.0	86	0.31	54
3	43	0.16	42
3.5	**50**	**0.20**	**45**
	Reference		
	50	…	44

TABLE III. Used unit-less pre-factors as a function of the three involved atom species in the interaction with (w.) or without (w/o) an impedance adaptation.

	With impedance adaptation		Without impedance adaptation	
Basis	A	λ	A	λ
C/C/C	7.05	150	7.05	150
GeTe/GeTe/GeTe	3.5	21	3.5	21
GeTe/C/*[a]	3.5	21	5.28	85.5

[a]Placeholder for GeTe or C.

The decrease of anisotropy is visible in the dispersion relations shown in Fig. 3. Indeed, there are fewer modes in the in-plane direction for longitudinal polarization and a wave number of 1.0 $Å^{-1}$ for the smooth interface superlattice. The wave vector at which it occurs is halved when the thickness of $a-C$ is doubled (around 0.5 $Å^{-1}$). This depletion of mode density disappears when roughness is introduced. The effect is, thus, probably due to a resonant mode or coupling with transverse modes that are destroyed by the roughness. However, the wavelengths concerned (0.6 or 1.2 nm) are not multiple of the superlattice period or thicknesses, and this effect is limited to the in-plane direction so that this is not a Bragg mirror effect. Similar depletion appears for transverse polarization in the in-plane direction for $t_{a-C} = 1$ nm (a-C layer thickness) but is not present for an amorphous layer thickness of 2 nm. In this case, the phenomenon could be linked to resonance modes that are destroyed by the roughness.

The mean free path (MFP) as a function of wavelength is displayed in Fig. 4. These MFPs are computed via the attenuation of the amplitude of a wave-packet propagating in the sample at 0 K shown in Fig. 15 of Appendix B 2, and the wavelength is inferred from the dispersion of GeTe extracted for the respective polarizations (see Appendix B 2 for details). The vertical blue lines indicate where the wavelength corresponds to multiple GeTe thicknesses. They serve as guides to identify an eventual coherent effect due to the periodicity.

A first observation is that for all configurations, the MFP increases with the wavelength, as expected for crystalline–amorphous nanocomposites.[42] There is no sharp decrease in MFP for $\lambda = t_{GeTe}/n$ with n being an integer. This shows again that the

19 December 2023 12:28:58

Published under an exclusive license by AIP Publishing

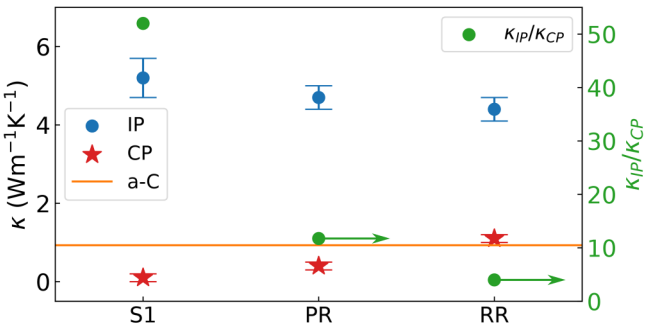

FIG. 2. In-plane (IP represented by blue dots) and cross-plane (CP represented by red stars) thermal conductivity of the nanocomposites without impedance adaptation (left axis) and anisotropy for each sample (green dots reporting to the right axis). The thermal conductivity of the bulk amorphous phase is given as a reference by the orange line.

Bragg mirror effect is either unimportant or not observable with this method due to coherence length considerations, the wavepacket being too short to interact with itself after reflection.[10] The roughness seems to increase the MFP for a large wavelength, in particular, for the transverse polarization. This is consistent with the increase of κ_{CP}. The periodicity of the roughness does not affect the MFP beyond uncertainty. However, we cannot rule out an effect on κ that would be smaller than the uncertainty.

For the in-plane direction, the situation is different and the behavior of longitudinal and transverse polarizations differs. Most interestingly, for the transverse polarization, periodic roughness increases the MFP for wavelengths from 2 nm on, while random roughness has no impact. This effect is discussed more in depth for the potential with impedance adaptation (see Sec. IV). For the longitudinal polarization, there is no change between the different configurations. The roughness has no impact, and the propagation in the crystal dominates. The MFP does not monotonously increase

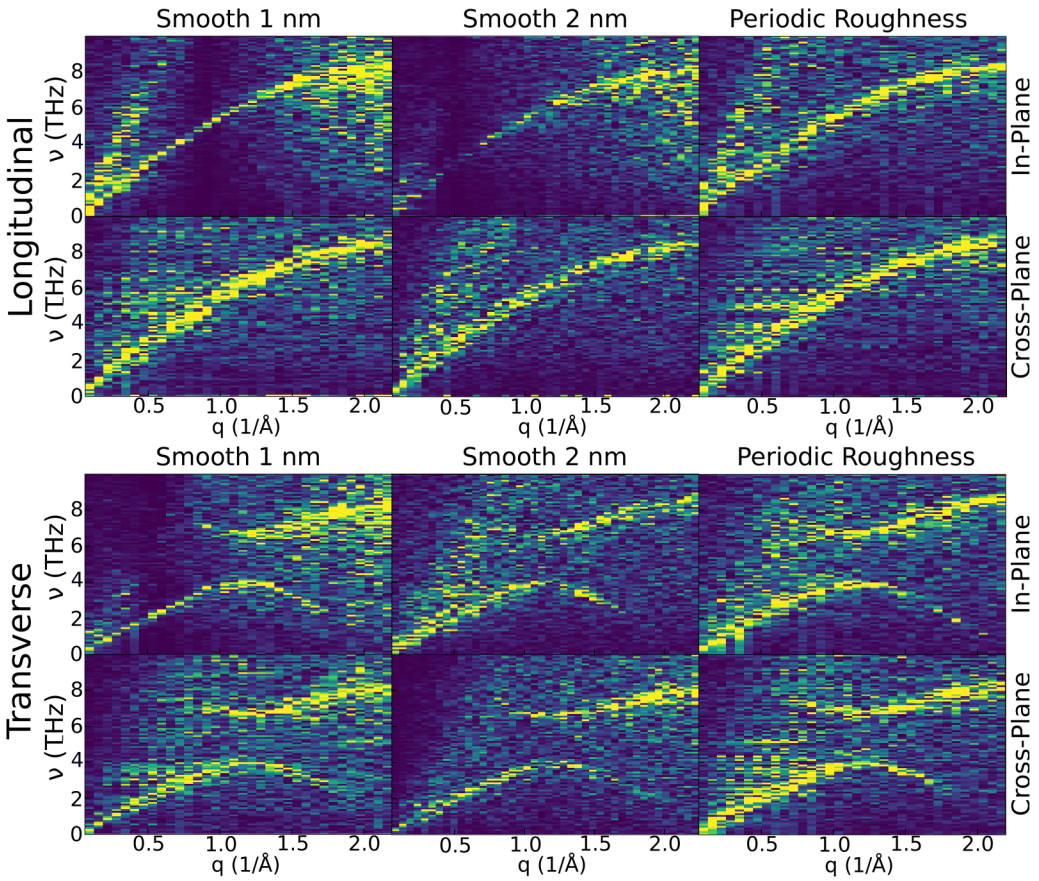

FIG. 3. Dynamical structure factor for the smooth superlattice with simple and double amorphous layer thicknesses and the superlattice with the periodic roughness without impedance adaptation for the longitudinal (top) and transverse (bottom) polarizations. The colors report the normalized intensity of the mode to outline the dispersion.

19 December 2023 12:28:58

Published under an exclusive license by AIP Publishing

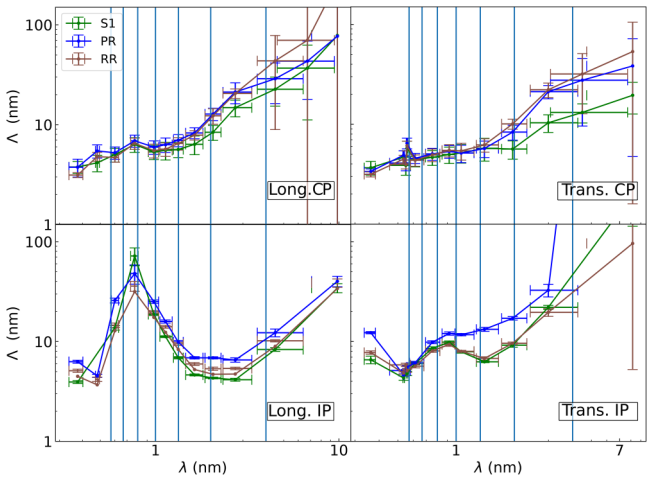

FIG. 4. MFP (Λ) longitudinal (left), transverse (right) in the cross-plane (top row) and in-plane (bottom row) direction of the nanocomposites without impedance adaptation; it is given as a function of the wavelength in GeTe. The vertical blue lines correspond to the value for which $\lambda = t_{GeTe}/n$ with n an integer and t_{GeTe} the GeTe layer thickness to check for Bragg conditions.

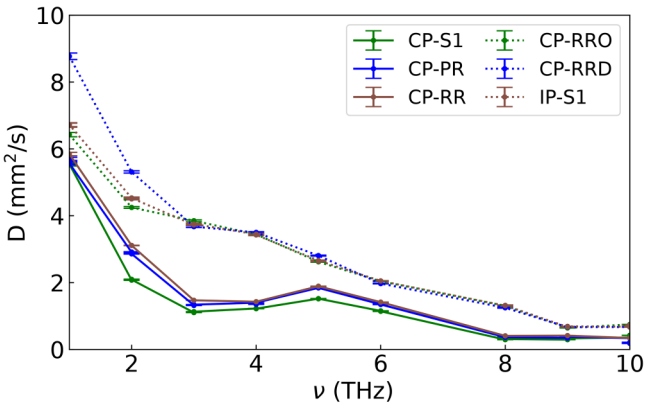

FIG. 5. Thermal diffusivity as a function of frequency of the nanocomposites without impedance adaptation. The full lines give the in-plane diffusivity and the dashed line the cross-plane one.

with the wavelength. Instead, it has a maximum at around 0.8 nm, which corresponds to the bandgap for transverse phonons as previously reported.[42]

The thermal diffusivity characterizes the transmission of non-coherent excitations. For fully amorphous samples, this allow one to measure the contribution of diffusons to the thermal conductivity.[28,43] In Fig. 5, it appears that for all superlattices, the thermal diffusivity is noticeably higher in the in-plane direction, and this is consistent with the decrease of κ_{CP} due to the interface. In the in-plane direction, all the configurations exhibit similar thermal diffusivity, and the only exception is the periodic roughness (PR) that seems to have comparatively higher diffusivity at low frequency. This increase might be linked to the MFP increase observed for the transmission of transverse wave-packets. In the cross-plane direction, the thermal diffusivity decreases from 1 to 3 THz and then re-increases to have a maximum at 5 THz. This non-monotonous behavior has already been observed for a-Si/c-Si nanocomposites[28,44] and has been linked to the end of the transverse phonon branch. This is consistent with what was observed in the transverse DSF in Fig. 3. It appears clearly that the transverse acoustic branch has a maximum at 4 THz. Finally, for the cross-plane direction, the roughness seems to increase the thermal diffusivity. This is consistent with the increase of thermal conductivity reported earlier.[5]

As a conclusion, we have seen that without impedance adaptation, the roughness increases κ_{CP} and decreases κ_{IP}. These observations are consistent with the literature, in particular, when there is only a mass difference between the layers.[6] The increase of thermal diffusivity for the cross-plane direction is consistent with the increase of thermal conductivity κ_{CP}. Surprisingly, periodic roughness induces a large increase in the MFP of transverse phonons in the in-plane direction. Finally, the study of the DSF showed that for smooth interfaces, resonance effects induce a wave-vector bandgap in the in-plane direction, which gives rise to a maximum of the longitudinal phonon mean free path in this direction.

IV. PROPERTIES OF THE NANOCOMPOSITES WITH IMPEDANCE ADAPTATION

To deal with interactions between species, a more common approximation is to use the average values of the parameters used for the individual species to model the interaction.[29] This is the approach considered in this section. Here, all the geometries appearing in Fig. 1 are studied.

Let us first start with the thermal conductivity, κ_{CP} and κ_{IP}, which are displayed in Fig. 6. It first appears that the configuration with doubled a-C thickness is the only one with both an in-plane and a cross-plane reduction of the thermal conductivity, and this is expected as the relative importance of the a-C layer is increased.[45] The anisotropy is also much smaller than without impedance adaptation in Fig. 2, with a factor of almost 20 in the case of the smooth SL. κ_{CP} is much higher than previously for all the configurations, and the adaptation of impedance at the GeTe–C interface seems to decrease the role of the interface. As a result, κ_{CP} remains larger than the value in bulk a-C (excepted when the amorphous layer thickness is doubled). This decreased interfacial phonon scattering is also visible through the diminished impact of roughness, which does not increase κ_{CP}. For the configuration with random roughness, it is even slightly decreased. However, this might be due to the proximity of the a-C layers when the two directions of roughness are opposed [see Fig. 1(c)]. Changing the relative orientation of the crystalline layers does not affect κ_{CP} either. This suggests that there is no phonon tunneling from one crystalline layer to the next, which would be impeded by the orientation change. The diffusion of C in the GeTe layers decreases κ_{IP}, which can be understood as due to the additional scattering from carbon substitutions within the GeTe layer. Finally, roughness seems to increase κ_{IP}, but this

19 December 2023 12:28:58

Published under an exclusive license by AIP Publishing

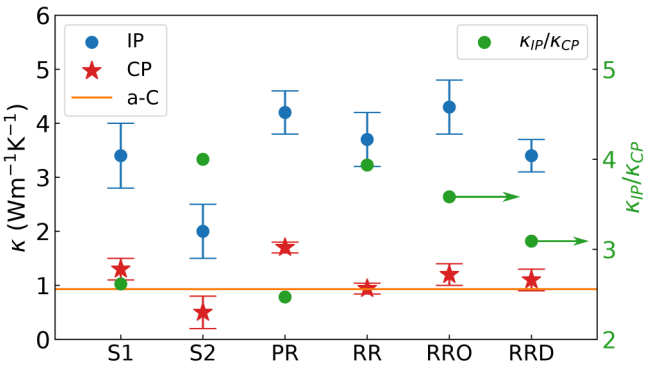

FIG. 6. In-plane (IP represented by blue dots) and cross-plane (CP represented by red stars) thermal conductivity of the nanocomposites with impedance adaptation (left axis) and anisotropy for each sample (green dots reporting to the right axis). The thermal conductivity of the amorphous phase is given as a reference by the orange line.

remains within the uncertainty. The only configuration that has a decreased κ_{IP} is that with increased amorphous layer thickness, this variation can be understood by the increased importance of the a-C layer.

The DSFs in the in-plane and cross-plane directions are depicted in Fig. 7. Contrary to Fig. 3, no mode depletion appears, confirming that the average parameters in the C–GeTe interaction decrease the impedance mismatch and prevents a standing wave to form. Without these bandgaps, the only effect of doubling t_{a-C} on the DSF is that the branches of a-C appear more clearly. Finally, roughness seems to increase the dispersions width, in particular, in the longitudinal direction and the transverse polarization for the cross-plane direction. As this dispersion width increase corresponds to increased phonon attenuation, this is consistent with the increased disorder.

After studying the dynamical structure factor, we can focus on the energy transmission as a function of wavelength for the different polarizations and orientations, starting with the cross-plane direction in Fig. 8. As in Fig. 4, the MFP increases with wavelength.

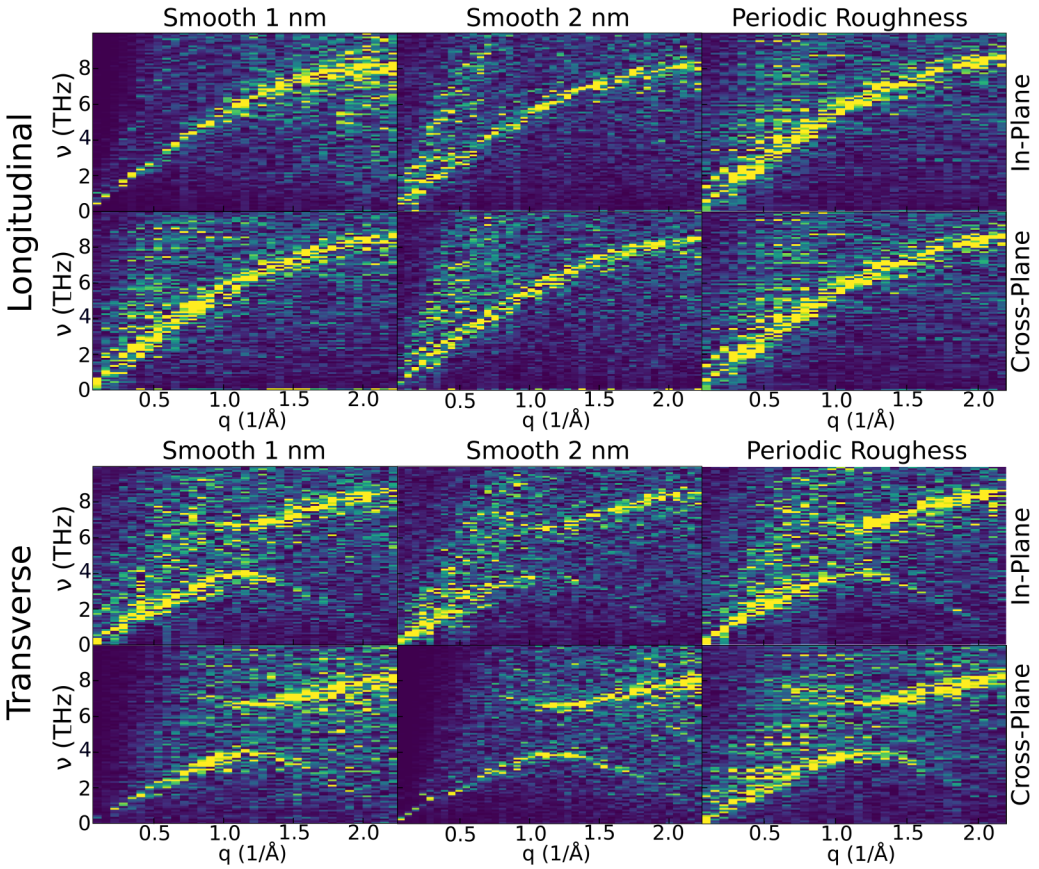

FIG. 7. Dynamical structure factor for the smooth superlattice with t_{a-C} 1 or 2 nm and the superlattice with the periodic roughness with impedance adaptation for the longitudinal (top six panels) and transverse (bottom six panels) polarizations. The colors report the normalized intensity of the mode to outline the dispersion.

19 December 2023 12:28:58

Published under an exclusive license by AIP Publishing

For the longitudinal direction, no clear change between configuration is observed for the MFP. For the transverse direction, the roughness increases the transmission, in particular, when randomness is introduced. This is consistent with previous studies.[5] This effect seems to disappear when the crystalline orientation is alternated between the layers. The interdiffusion of C has no effect on the transmission. Indeed, due to the way the diffusion of carbon is modeled, it has a negligible cross section in the cross-plane direction. As a reminder, this choice was made to reproduce the effect of diffusion of carbon in grain boundaries. There are no obvious links between the variations of MFP observed in Fig. 8 and κ_{CP}. In particular, no distinction can be made between periodic and random roughness that seemed to induce the opposite effect on thermal conductivity.

Concerning the MFP in the in-plane direction, also reported in Fig. 8, we find also in this case the presence of a maximum for wavelengths around 0.8 nm, which can be attributed to the maximum of the transverse branch.[42] As this maximum appears at high frequencies, it is sensitive to the presence of small defects, such as the insertion of C atoms in the crystalline part. This explains the dimming of this peak when carbon atoms are introduced in GeTe. One can also note that the random roughness also decreases this effect.

In the transverse direction, the MFP is considerable at a low wave number, much larger than the size of the device. Moreover, as observed in Sec. III, the MFP in the case of periodic roughness is notably larger for a wide range of wavelength. To investigate this phenomenon, a representation of the kinetic energy of the atoms during the propagation of 2 THz transverse impulsion in the in-plane direction in a cross section is shown in Fig. 9. Using this representation, one can clearly see the different phenomena occurring during wave-packet propagation. First, the energy is mainly located on the GeTe atoms, with little to no energy in the a-C layers. This is consistent with a decreased transmission in the amorphous phase. The wave-packet travels through the sample, and it is particularly visible for the periodic roughness in the central column. At this frequency, the wavelength is of 1.5 nm, and thus, waves are clearly visible as vertical stripes in the figure. Then, after the passage of the wave-packet, an energy trail subsists. This is the part of the energy that is scattered by the interfaces, and it appears to be much larger for the smooth and random roughness interfaces. This decreased attenuation is, thus, linked to the roughness periodicity. However, it does not depend strongly on the wavelength, as it spans over λ values going from 0.8 to 2 nm.

Last, the diffusivities are displayed in Fig. 10. Again, the diffusivities are larger in the in-plane direction. In this direction, the peak at 5 THz observed in Fig. 5 is visible, and only the orientation change decreases the thermal diffusivity at low frequencies. This can be interpreted as a decrease of the transmission of the low frequencies through the sample. Contrary to what was already observed without impedance adaptation, smooth interfaces do not have lower thermal diffusivity. The adaptation of the impedance at the C–GeTe interface seems to decrease the scattering at the interface. In the in-plane direction, the same increase of thermal diffusivity at low frequencies for the periodic roughness as in Fig. 5 is observed. Smooth and random roughness interfaces have very similar properties. Finally, the interdiffusion of carbon in the GeTe decreases the thermal diffusivity from 2 to 8 THz, similar to what already observed in Fig. 8.

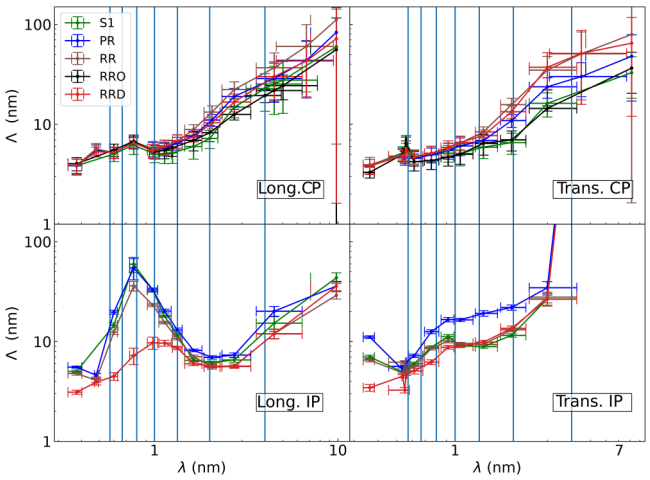

FIG. 8. MFP (Λ) longitudinal (left), transverse (right) in the cross-plane (top row) and in-plane (bottom row) direction of the nanocomposites with impedance adaptation; it is given as a function of the wavelength in GeTe. The vertical blue lines correspond to the value for which $\lambda = t_{GeTe}/n$ with n an integer to check for Bragg conditions.

To conclude, we have observed that the impedance adaptation decreases the role of the interfaces as a scattering source on the thermal conductivity. The crystalline orientation only impacts marginally the thermal diffusivity, and the diffusion of carbon decreases the in-plane MFP and seems to affect the thermal

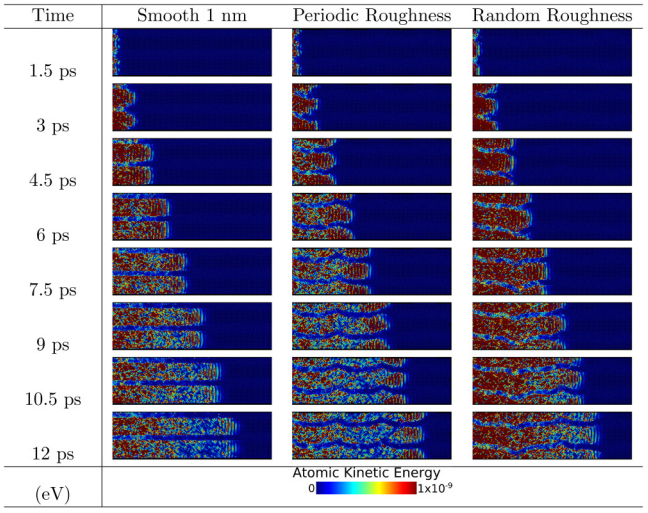

FIG. 9. Cross-sectional view of a transverse polarized wave-packet at 2 THz ($\lambda = 1.2$ nm) going through the superlattice in-plane direction with impedance adaptation.

19 December 2023 12:28:58

Published under an exclusive license by AIP Publishing

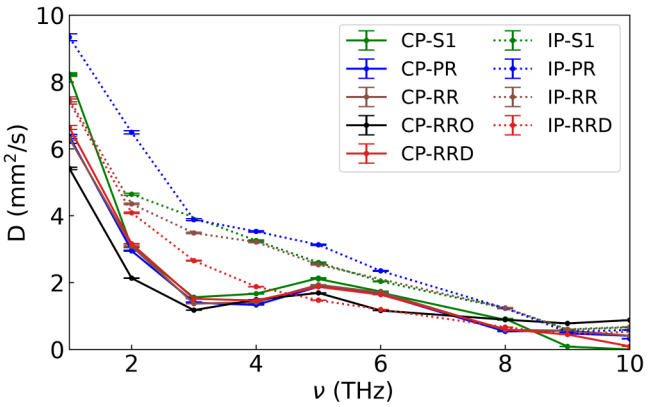

FIG. 10. Thermal diffusivity as a function of frequency of the nanocomposites with impedance adaptation. The full lines give the in-plane diffusivity and the dashed line the cross-plane one.

conductivity. Finally, again, the periodicity increases the transmission of transverse phonons in the in-plane direction.

V. DISCUSSION AND CONCLUSION

We have studied the thermal and vibrational properties of GeTe/a-C superlattices. For this, the SW interatomic potential, with tuned masses and bond stiffness, has been used. This allows an approximate reproduction of the impedance ratio (see Appendix A). While imperfect with regard to network topology, it still allows studying a superlattice composed of alternating layers of a stiff and light amorphous material and a comparatively soft and heavy crystal layer. To model the interaction between C and GeTe within this simplified model, two different approaches are used. Either using the properties of GeTe creating an abrupt transition between the soft GeTe and the stiff C (that is, no impedance adaptation) or using the arithmetic mean of the parameters used for GeTe and C creating a smoother transition between the material properties at the interface, that is, impedance adaptation.

Our findings show that the modeling choice of the interaction between the layers impacts the sensitivity to roughness. Without impedance adaptation, the roughness decreases the in-plane thermal conductivity κ_{IP} and increases the cross plan one κ_{CP} as predicted in the literature.[5,6,27] The effect is even more important for random roughness, though it might be linked to the closeness of the amorphous layers through the periodic boundary conditions [see Fig. 1(c)]. On the contrary, with impedance adaptation, no distinction between the configurations can be made, their properties being similar. The lack of impact of the roughness can be attributed directly to the adaptation of impedance. This result could not be observed in previous studies, where only masses were modified to recreate the impedance mismatch or in studies where the arithmetic average of the parameters of each species to model the interfacial interaction was used, but the role of roughness was not studied.[10,46]

The layer thickness/periodicity has been indirectly studied through the variation of the amorphous layer thickness. As expected, the thermal conductivity decreases as the thickness increases.[45] A parallel can be made with crystalline superlattices, where for very low thicknesses, the cross-plane thermal conductivity decreases as the layer thickness increases due to coherent phonon scattering.[9] However, in the present study, because only the amorphous layer thickness is increased, we cannot attribute the effect solely to an eventual coherent effect. Moreover, as visible in Fig. 13, there is a strong mode mismatch between the layers, making transmission unlikely.

Having a different orientation in the crystalline layers affects the thermal diffusivity, but not enough to impact κ_{CP}. Finally, the diffusion of C in GeTe layers reduces the MFP and thermal diffusivity in the in-plane direction and marginally κ_{IP}. As a final remark on the thermal conductivity, one can note that the anisotropy is much higher without impedance adaptation and increased by thicker amorphous layers. This is interesting to note because in the context of phase change memory, thermal anisotropy can be useful as it could allow heat penetration in the depth of the material while not affecting the next bit.[47]

The study of the mean free path and thermal diffusivity showed clearly that the roughness increases the cross-plane transmission, in particular, for the transverse polarization. This is consistent with the increase of κ_{CP} without impedance adaptation. In the in-plane direction for the longitudinal polarization, the MFP is not influenced by roughness. On the contrary, for the transverse polarization, periodic roughness increases significantly the MFP, independently of the modeling of the interface interactions. This is also true for the in-plane thermal diffusivity. Both these increases are likely related only to the crystalline contribution and not to an interaction with the amorphous phase, as they do not depend on the interface modeling.

The link between the mean free path/thermal diffusivity and the thermal conductivity remains unclear. An explanation for this is the role of phonon–phonon scattering that increases with the temperature so that the observation made at 0 K with the wave-packet simulations may not hold at 300 K. Moreover, only two directions of propagation have been investigated, in-plane and cross-plane. Other phenomena might arise for other orientations that are not orthogonal to the SL layers, especially when roughness is introduced.

In this work, we have assumed Gaussian roughness; however, it is important to note that the shape of the roughness may impact the properties of the interface.[5,48] Another important finding of this paper is that paying attention to the interface roughness is not enough, and the type of interaction at the interface does matter. This has been achieved through an *ad hoc* change of the interatomic potential parameters, but interaction at the interface could also be tuned through surface functionalization, as described for water at the surface of silica.[49] However, it is to be noted that due to the copy and paste method used here, we do not expect to observe self-assembly in our simulations, and it is not observed experimentally.[17]

Finally, if no bandgap resulting from the Bragg mirror effect is observed in the cross-plane direction, in the absence of impedance adaptation, modal depletion appears in the in-plane direction. As the wavelength being depleted is dependent on the amorphous layer thickness, it is probably due to in-plane/cross-plane coupling in this layer.

19 December 2023 12:28:58

Published under an exclusive license by AIP Publishing

Overall, without impedance adaptation, the anisotropy is stronger and more dependent on the roughness properties. These have two origins: the large difference in elastic properties between the two materials and the abrupt transition between the two materials. The latter appears to be important, as most of these behaviors and properties disappear when introducing adaptation of impedance at the interface by modifying the inter-species properties. While being an arbitrary choice, the latter appears as more realistic than a sharp transition from one material to the other. It is worth noticing that such adaptation is not possible when changing the mass only of the atoms,[5,27] and such modeling probably enhances the effect of the interface.

To conclude, we have developed a simple model to study amorphous crystalline superlattices. Using two different sets of interaction potentials, we investigated the role of impedance adaptation, which has been disregarded in superlattice simulations up to now. We have shown that the anisotropy and the impact of roughness on the thermal properties depend strongly on the interface properties. In the absence of impedance adaptation at the interface, the anisotropy is very high, and the roughness impacts the thermal properties. The introduction of impedance adaptation between the layers essentially destroys these effects, and the thermal conductivity depends much less on the roughness. The increased role of interfaces is also seen through the presence of depletion of the acoustic modes in the in-plane direction without impedance adaptation. Finally, using wave-packet propagation, we have seen that the MFP is also affected by the roughness periodicity that increases it for transverse phonons in the in-plane direction. These findings highlight the importance of the interaction at the interface on the thermal properties and can inform the design of future models using more realistic interaction potentials.

ACKNOWLEDGMENTS

This work was granted access to the HPC resources of IDRIS under the allocation 2021- A0110911092, made by GENCI. This research was funded by ANR under the contract MAPS ANR-20-CE05-0046-03 and from the AURA region for the NanoCHARME project. The authors also thank the CNRS for funding the mobility of J.-Y.R. to Lyon through the Dialogue program. The authors want to thank fruitful discussions with Anne Tanguy.

AUTHOR DECLARATIONS

Conflict of Interest

The authors have no conflicts to disclose.

Author Contributions

Paul Desmarchelier: Conceptualization (equal); Data curation (equal); Formal analysis (equal); Investigation (equal); Methodology (equal); Writing – original draft (equal). **Valentina M. Giordano:** Funding acquisition (equal); Methodology (equal); Project administration (equal); Supervision (equal); Writing – review & editing (equal). **Jean-Yves Raty:** Methodology (equal); Writing – review & editing (equal). **Konstantinos Termentzidis:** Conceptualization (equal); Funding acquisition (equal); Methodology (equal); Project administration (equal); Supervision (equal); Writing – review & editing (equal).

DATA AVAILABILITY

The data that support the findings of this study are available from the corresponding author upon reasonable request.

APPENDIX A: PROPERTIES OF BULK a-C AND GeTe WITH THE *AD HOC* POTENTIAL

In this section, the properties of the modeled GeTe and a-C are studied. First, the radial distribution function (RDF) is displayed in Fig. 11. It first appears that the modeled GeTe retains the RDF of the original potential, which was expected given that only the prefactor is modified. For the amorphous phase, however, the RDF differs from the one a-Si, meaning using a stiffer 3 body interaction impacts significantly the structure. The first neighbor is brought closer, and the second neighbor shell is sharper.

Both vibrational density of states (VDOS, see Appendix B 3) are displayed in Fig. 12. It appears that the VDOS of GeTe is very similar to that of crystalline silicon, with the different characteristic peaks. However, it is compacted from 0 to 8 THz, instead of spanning from 0 to 19 THz.[32] This can be explained by the weaker two-body interaction and heavier atoms both contributing to a red shift. For a-C, no distinctive peaks can be recognized, and the VDOS is very different from the one of a-Si.[45] It is worth mentioning that both the VDOS obtained are very different from those expected for GeTe[50] and a-C[51] due to the simplified modeling approach taken.

The study of the vibrational properties can be pursued with the study of the dynamical structure factor. In Fig. 13(a), the one of GeTe in the ΓX direction of the Brillouin zone in the longitudinal and transverse polarization is displayed. It is very close to that of c-Si, but once again compressed to a smaller frequency range.[42] The blurred vertical lines are numerical artifacts. For a-C, the

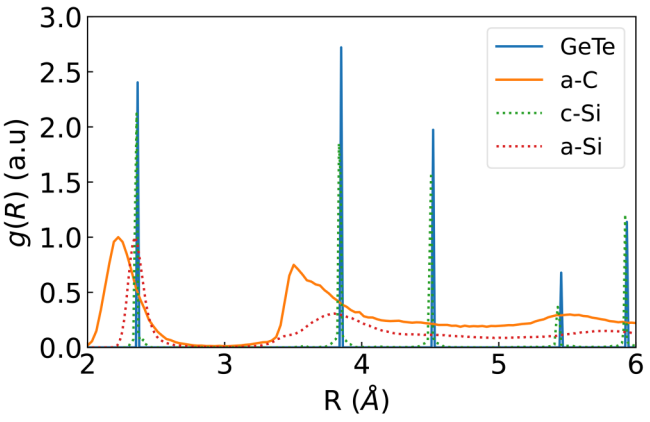

FIG. 11. Radial distribution function for the modeled a-C and GeTe as well as the RDF for the pristine material.

19 December 2023 12:28:58

Published under an exclusive license by AIP Publishing

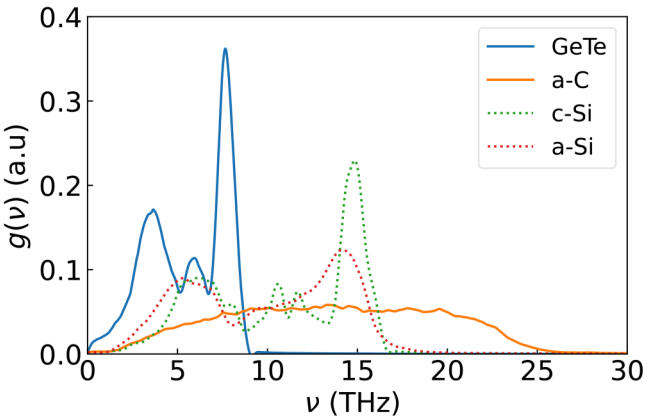

FIG. 12. Vibrational density of states of the bulk a-C and GeTe modeled, compared to the one of a-Si and c-Si for the original unmodified potential.

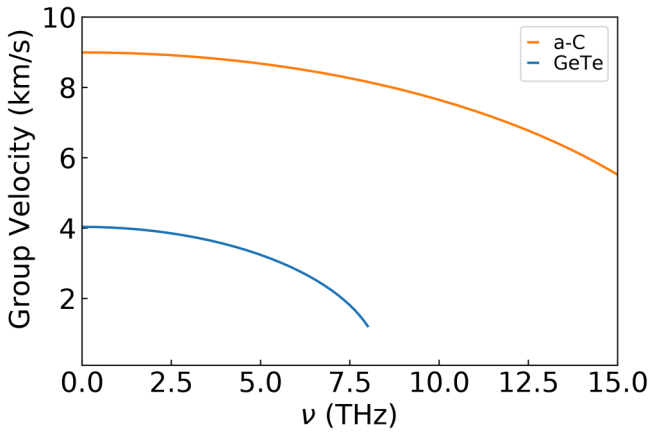

FIG. 14. Longitudinal group velocities of the modeled a-C and GeTe extracted from the DSF.

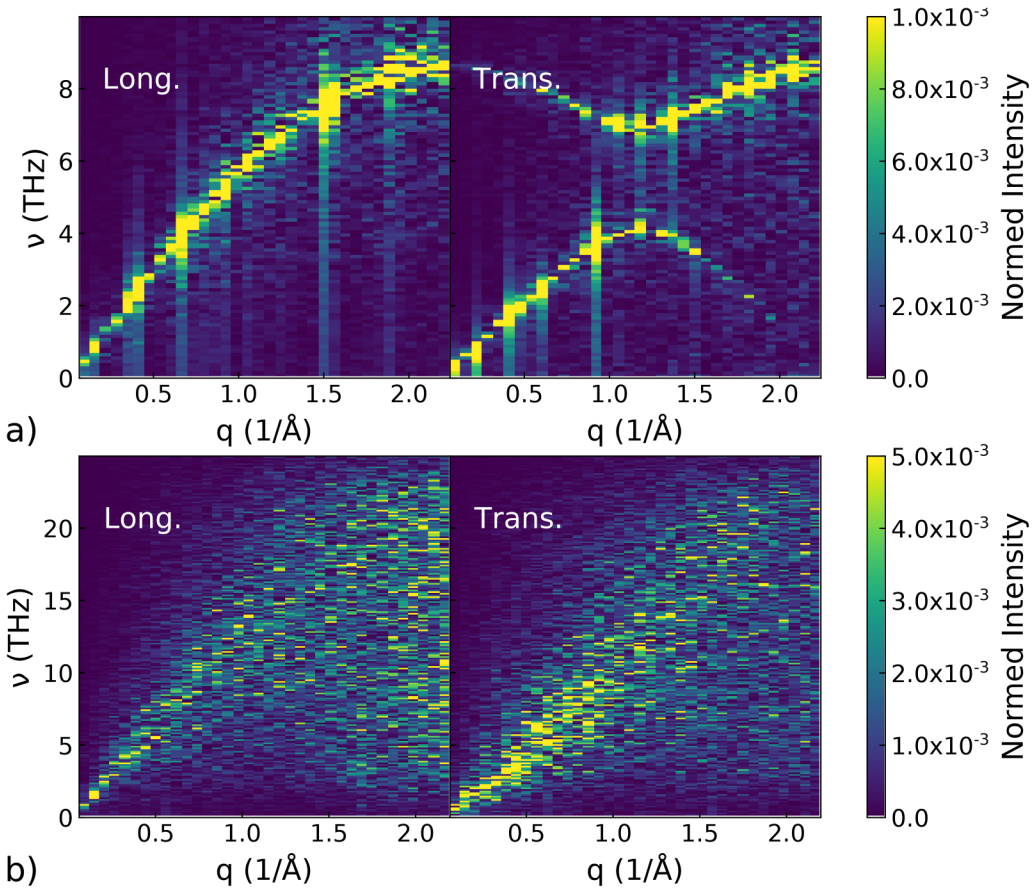

FIG. 13. Dynamical structure factor of (a) the GeTe in the ⟨100⟩ (ΓX) direction and (b) the modeled a-C.

19 December 2023 12:28:58

Published under an exclusive license by AIP Publishing

TABLE IV. Thermal conductivity of reference and thermal conductivity obtained. For GeTe, the reference value is taken from Samanta *et al.*,[53] and for a-C of density 2.5 g cm^{-3}, the results are taken from Bullen *et al.*[35]

	Ref (W m^{-1} K^{-1})	SW (W m^{-1} K^{-1})
κ_{latt} a-C	≈1	0.93
κ_{latt} GeTe	≈2.8	44

dispersion lines are much thicker and blurred in comparison with the unmodified potential case, which is a sign of strong attenuation.[52]

The group velocity can be derived from the dispersion relations observed on the dynamical structure factor. They are obtained thanks to a fit of the maximum for each point in the region of the branch to a sine function. The derivative of this function can then be computed to obtain the group velocity, which is displayed in Fig. 14. The values of the group velocity at 0 THz can be compared to the sound velocity obtained in the literature: 1.9 km s^{-1} for α-GeTe,[38] which is much lower than the 4 km s^{-1} obtained here. This difference is probably due to the peculiar structure of GeTe, as 4 km s^{-1} corresponds to the group velocity obtained through the elastic properties. Then, for a-C, we get a group velocity of 9 km s^{-1}, which is lower than the 14.5 km s^{-1} obtained using the formula $\left(v \approx \frac{K+4/3G}{\rho}\right)$ using the data from the work of Jana *et al.*[39] Even if the impedance values and ratio are underestimated, the model can still be useful to study qualitatively superlattices composed of a soft and heavy crystalline layer and a stiff light amorphous layer.

The thermal conductivity of the modeled materials is listed in Table IV. Despite the disagreement in terms of speed of sound, the thermal conductivity of a-C is close to that of Bullen *et al.*[35] However, for GeTe, the thermal conductivity is much higher than the expected value. Again, this disagreement can be explained by the model interatomic potential and structure that does not reproduce the band structure of GeTe.

APPENDIX B: METHODS

1. Equilibrium molecular dynamic

The equilibrium molecular dynamics (EMD) method is used to estimate the thermal conductivity of the different configurations. It is based on the fluctuation–dissipation theorem, which links the decay of the fluctuations of an internal variable to its response function. For the thermal conductivity, the flux auto-correlation integral is linked to the thermal conductivity using the Green–Kubo formula

$$\kappa_{\alpha\beta} = (Vk_BT^2)^{-1} \int_0^\infty \langle J_\alpha(0) J_\beta(t) \rangle \, dt, \tag{B1}$$

with α and β being the directions, V the volume of the system, k_b the Boltzman constant, and $J_\beta(t)$ the thermal flux in the direction β at a time t.[54]

The configurations are first heated at 50 K using a random initial velocity distribution. After that, the temperature is increased from 50 to 600 K at constant pressure in 0.05 ns. Then, the system is annealed at 600 K with a Nosé–Hoover thermostat for 0.25 ns. After this annealing, the temperature is decreased to 300 K at constant pressure in 0.05 ps and then equilibrated at 300 K for 1 ns. The flux auto-correlation function is measured after these equilibrating steps during 15 ns without a thermostat. For all the simulations, a time step of 5×10^{-1} fs is used. For the computation of the auto-correlation, the flux is sampled every 10 fs and the flux auto-correlation decay is computed over 0.04 ns. These simulations are repeated five times with a different initial velocity distribution for each repetition to get better statistics. The final value is the mean κ across the simulations, and the uncertainty range is defined by the extrema of the distribution.

2. Wave-packet propagation

The energy propagation in the superlattice can also be studied through the propagation of wave-packets. The method used here is very similar to the method used in a previous study.[42] An impulsion at a given frequency is imposed on a 2 Å slice in the middle of a GeTe slice, and the resulting energy propagation is monitored. The wave-packet is generated through a Gaussian windowed sinusoidal force excitation,

$$f = A\sin[2\pi\nu(t - 3\tau)] \exp\left[-\frac{(t - 3\tau)^2}{(2\tau^2)}\right], \tag{B2}$$

imposed to the atoms in the excited layer. The amplitude A is of 3.773×10^{-4} eV Å^{-1}. This is chosen low enough to only consider the geometrical effects and avoid anharmonicity. The spreading of the Gaussian window τ is chosen to be small enough to offer a compromise between the spatial extension of the wave-packet compared to the system length and the resolution in the frequency space. The used value is 0.72 ps.

In these simulations, the impulsion is the only source of movement, the initial velocities are set to 0, and the system is at mechanical equilibrium. The simulations are done at constant energy (once the excitation is done), with a time step of 1×10^{-3} ps.

To obtain a model that is large enough to compute the MFP, seven simulation boxes described in Sec. II A are needed. For the smooth or periodic roughness cases, the boxes are simply repeated in the in-plane or cross-plane direction. For the cases with random roughness, the seven different cases are placed back to back, as displayed in Fig. 15.

3. VDOS

The vibrational density of state (VDOS) is evaluated through the Fourier transform of the velocity auto-correlation function (VACF).[55] To this end, the system is first equilibrated at 300 K for 100 ps with a Nosé–Hoover thermostat. After this, the thermostat is switched off, and the system evolves at constant energy. Over this 100 ps long simulation, the VACF averaged over the particles. To get the VDOS, the Fourier transform of the VACF is finally computed and filtered using a Savitzky–Golay[56] polynomial filter.

19 December 2023 12:28:58

Published under an exclusive license by AIP Publishing

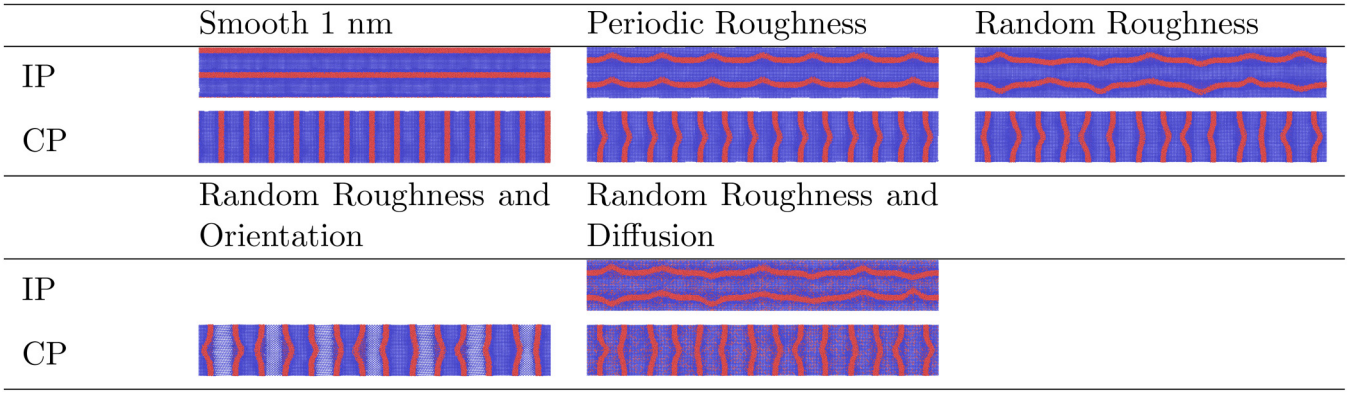

FIG. 15. The different configurations for the study of transmission of wave-packets at low temperature.

4. Dynamical structure factor

The dynamical structure factor (DSF) is a spatial and temporal Fourier transform of the atomic displacements used to characterize the vibrational properties of a system. This is similar to what can be measured by x ray or by neutron scattering experiments.[57] It is computed with the same method as in a previous publication.[58] First, the sample is heated to 300 K and equilibrated at this temperature for 50 ps using a Nosé–Hoover thermostat. After this, the atomic trajectories are recorded during a 10 ps long constant energy simulation, the position being recorded every 1×10^{-2} ps. Then, the DSF is computed using the following expression:

$$S(\mathbf{q}, \omega) = \frac{2}{NT}\left|\sum_{i}^{N_{at}} \exp(-i\mathbf{q}\cdot\mathbf{r_i}) \int_0^{\tau} \mathbf{u_i}(\mathbf{r_i}, t)\mathbf{m_\eta}\exp(i\omega t)\, dt\right|^2, \quad \text{(B3)}$$

with $\mathbf{q}$ being the wave vector, $\mathbf{u_i}$ and $\mathbf{r_i}$ the displacement and position of the ith atom, m_η the polarization vector (parallel or perpendicular to $\mathbf{q}$), T the temperature, and N the total number of atoms.[59] The DSF can be obtained for the different vectors of the Brioullin zone. Here, $\mathbf{q}$ is either perpendicular to the interfaces (the cross-plane) or parallel to the interfaces (in-plane). From the DSF, the phononic dispersion curves can be obtained. For this, the DSF is first filtered through a convolution with a typical energy resolution curve of linewidth 0.33 THz (as suggested by Tlili *et al.*[28]). Then, for a given wave-vector direction, the dispersion is estimated from the frequency for which the DSF has the highest value for each wave vector within the acoustic phonon frequency range. Once each wave vector has a value, the curve is filtered using a Savitzky–Golay polynomial filter.

REFERENCES

[1]M. Le Gallo and A. Sebastian, "An overview of phase-change memory device physics," J. Phys. D: Appl. Phys. **53**, 213002 (2020).
[2]R. A. Kishore and S. Priya, "A review on low-grade thermal energy harvesting: Materials, methods and devices," Materials **11**, 1433 (2018).
[3]E. S. Landry and A. J. H. McGaughey, "Effect of interfacial species mixing on phonon transport in semiconductor superlattices," Phys. Rev. B **79**, 075316 (2009).
[4]J. Maire, R. Anufriev, R. Yanagisawa, A. Ramiere, S. Volz, and M. Nomura, "Heat conduction tuning by wave nature of phonons," Sci. Adv. **3**, e1700027 (2017).
[5]K. Termentzidis, S. Merabia, P. Chantrenne, and P. Keblinski, "Cross-plane thermal conductivity of superlattices with rough interfaces using equilibrium and non-equilibrium molecular dynamics," Int. J. Heat Mass Transf. **54**, 2014–2020 (2011).
[6]K. Termentzidis, P. Chantrenne, and P. Keblinski, "Nonequilibrium molecular dynamics simulation of the in-plane thermal conductivity of superlattices with rough interfaces," Phys. Rev. B **79**, 214307 (2009).
[7]B. Qiu, G. Chen, and Z. Tian, "Effects of aperiodicity and roughness on coherent heat conduction in superlattices," Nanoscale Microscale Thermophys. Eng. **19**, 272–278 (2015).
[8]M. N. Luckyanova, J. A. Johnson, A. A. Maznev, J. Garg, A. Jandl, M. T. Bulsara, E. A. Fitzgerald, K. A. Nelson, and G. Chen, "Anisotropy of the thermal conductivity in GaAs/AlAs superlattices," Nano Lett. **13**, 3973–3977 (2013).
[9]J. Ravichandran, A. K. Yadav, R. Cheaito, P. B. Rossen, A. Soukiassian, S. Suresha, J. C. Duda, B. M. Foley, C.-H. Lee, Y. Zhu *et al.*, "Crossover from incoherent to coherent phonon scattering in epitaxial oxide superlattices," Nat. Mater. **13**, 168–172 (2014).
[10]B. Latour and Y. Chalopin, "Distinguishing between spatial coherence and temporal coherence of phonons," Phys. Rev. B **95**, 214310 (2017).
[11]M. Zacharias, J. Bläsing, P. Veit, L. Tsybeskov, K. Hirschman, and P. M. Fauchet, "Thermal crystallization of amorphous Si/SiO_2 superlattices," Appl. Phys. Lett. **74**, 2614–2616 (1999).
[12]L. Yang, B. Latour, and A. J. Minnich, "Phonon transmission at crystalline-amorphous interfaces studied using mode-resolved atomistic green's functions," Phys. Rev. B **97**, 205306 (2018).
[13]A. France-Lanord, S. Merabia, T. Albaret, D. Lacroix, and K. Termentzidis, "Thermal properties of amorphous/crystalline silicon superlattices," J. Phys.: Condens. Matter **26**, 355801 (2014).
[14]K. Termentzidis, A. France-Lanord, E. Blandre, T. Albaret, S. Merabia, J. Valentin, and D. Lacroix, "Thermal conductivity of regularly spaced amorphous/crystalline silicon superlattices. A molecular dynamics study," MRS Online Proc. Lib. **1543**, 71–79 (2013).
[15]P. Chen, N. A. Katcho, J. P. Feser, W. Li, M. Glaser, O. G. Schmidt, D. G. Cahill, N. Mingo, and A. Rastelli, "Role of surface-segregation-driven intermixing on the thermal transport through planar Si/Ge superlattices," Phys. Rev. Lett. **111**, 115901 (2013).
[16]D. Térébénec, N. Bernier, N. Castellani, M. Bernard, J.-B. Jager, M. Tomelleri, J. Paterson, M.-C. Cyrille, N.-P. Tran, V. M. Giordano, F. Hippert, and P. Noé,

19 December 2023 12:28:58

Published under an exclusive license by AIP Publishing

"Innovative nanocomposites for low power phase-change memory: GeTe/C multilayers," Phys. Status Solidi RRL **16**, 2200054 (2022).
[17]R. Chahine, M. Tomelleri, J. Paterson, M. Bernard, N. Bernier, F. Pierre, D. Rouchon, A. Jannaud, C. Mocuta, V. M. Giordano, F. Hippert, and P. Noé, "Nanocomposites of chalcogenide phase-change materials: From c-doping of thin films to advanced multilayers," J. Mater. Chem. C **11**, 269–284 (2022).
[18]G. Betti Beneventi, L. Perniola, V. Sousa, E. Gourvest, S. Maitrejean, J. Bastien, A. Bastard, B. Hyot, A. Fargeix, C. Jahan, J. Nodin, A. Persico, A. Fantini, D. Blachier, A. Toffoli, S. Loubriat, A. Roule, S. Lhostis, H. Feldis, G. Reimbold, T. Billon, B. De Salvo, L. Larcher, P. Pavan, D. Bensahel, P. Mazoyer, R. Annunziata, P. Zuliani, and F. Boulanger, "Carbon-doped GeTe: A promising material for phase-change memories," Solid-State Electron. **65-66**, 197–204 (2011).
[19]W.-D. Liu, D.-Z. Wang, Q. Liu, W. Zhou, Z. Shao, and Z.-G. Chen, "High-performance GeTe-based thermoelectrics: From materials to devices," Adv. Energy Mater. **10**, 2000367 (2020).
[20]J.-Y. Raty and M. Wuttig, "The interplay between peierls distortions and metavalent bonding in IV–VI compounds: Comparing GeTe with related monochalcogenides," J. Phys. D: Appl. Phys. **53**, 234002 (2020).
[21]D. Sarkar, S. Roychowdhury, R. Arora, T. Ghosh, A. Vasdev, B. Joseph, G. Sheet, U. V. Waghmare, and K. Biswas, "Metavalent bonding in GeSe leads to high thermoelectric performance," Angew. Chem. Int. Ed. **60**, 10350–10358 (2021).
[22]G. C. Sosso, G. Miceli, S. Caravati, J. Behler, and M. Bernasconi, "Neural network interatomic potential for the phase change material GeTe," Phys. Rev. B **85**, 174103 (2012).
[23]F. Li and J. S. Lannin, "Radial distribution function of amorphous carbon," Phys. Rev. Lett. **65**, 1905–1908 (1990).
[24]C. de Tomas, I. Suarez-Martinez, and N. A. Marks, "Graphitization of amorphous carbons: A comparative study of interatomic potentials," Carbon **109**, 681–693 (2016).
[25]F. H. Stillinger and T. A. Weber, "Computer simulation of local order in condensed phases of silicon," Phys. Rev. B **31**, 5262–5271 (1985).
[26]K. Termentzidis, P. Chantrenne, J.-Y. Duquesne, and A. Saci, "Thermal conductivity of GaAs/AlAs superlattices and the puzzle of interfaces," J. Phys.: Condens. Matter **22**, 475001 (2010).
[27]Y. Wang, C. Gu, and X. Ruan, "Optimization of the random multilayer structure to break the random-alloy limit of thermal conductivity," Appl. Phys. Lett. **106**, 073104 (2015).
[28]A. Tlili, V. M. Giordano, Y. M. Beltukov, P. Desmarchelier, S. Merabia, and A. Tanguy, "Enhancement and anticipation of the Ioffe–Regel crossover in amorphous/nanocrystalline composites," Nanoscale **11**, 21502–21512 (2019).
[29]J. Chen, G. Zhang, and B. Li, "Tunable thermal conductivity of $Si_{1-x}Ge_x$ nanowires," Appl. Phys. Lett. **95**, 073117 (2009).
[30]J. Tersoff, "Empirical interatomic potential for silicon with improved elastic properties," Phys. Rev. B **38**, 9902–9905 (1988).
[31]C. Fusco, T. Albaret, and A. Tanguy, "Role of local order in the small-scale plasticity of model amorphous materials," Phys. Rev. E **82**, 066116 (2010).
[32]R. Vink, G. Barkema, W. van der Weg, and N. Mousseau, "Fitting the Stillinger–Weber potential to amorphous silicon," J. Non-Cryst. Solids **282**, 248–255 (2001).
[33]M. Verdier, D. Lacroix, and K. Termentzidis, "Roughness and amorphization impact on thermal conductivity of nanofilms and nanowires: Making atomistic modeling more realistic," J. Appl. Phys. **126**, 164305 (2019).
[34]E. Blandre, L. Chaput, S. Merabia, D. Lacroix, and K. Termentzidis, "Modeling the reduction of thermal conductivity in core/shell and diameter-modulated silicon nanowires," Phys. Rev. B **91**, 115404 (2015).
[35]A. J. Bullen, K. E. O'Hara, D. G. Cahill, O. Monteiro, and A. von Keudell, "Thermal conductivity of amorphous carbon thin films," J. Appl. Phys. **88**, 6317–6320 (2000).
[36]K. Persson, (2014). "Materials data on GeTe (Sg:160) by materials project," DOE https://doi.org/10.17188/1272924.
[37]G. Clavier, N. Desbiens, E. Bourasseau, V. Lachet, N. Brusselle-Dupend, and B. Rousseau, "Computation of elastic constants of solids using molecular simulation: Comparison of constant volume and constant pressure ensemble methods," Mol. Simul. **43**, 1413–1422 (2017).
[38]R. Shaltaf, E. Durgun, J.-Y. Raty, P. Ghosez, and X. Gonze, "Dynamical, dielectric, and elastic properties of GeTe investigated with first-principles density functional theory," Phys. Rev. B **78**, 205203 (2008).
[39]R. Jana, D. Savio, V. L. Deringer, and L. Pastewka, "Structural and elastic properties of amorphous carbon from simulated quenching at low rates," Modell. Simul. Mater. Sci. Eng. **27**, 085009 (2019).
[40]S. Merabia and K. Termentzidis, "Thermal conductance at the interface between crystals using equilibrium and nonequilibrium molecular dynamics," Phys. Rev. B **86**, 094303 (2012).
[41]E. T. Swartz and R. O. Pohl, "Thermal boundary resistance," Rev. Mod. Phys. **61**, 605–668 (1989).
[42]P. Desmarchelier, A. Carré, K. Termentzidis, and A. Tanguy, "Ballistic heat transport in nanocomposite: The role of the shape and interconnection of nanoinclusions," Nanomaterials **11**(8), 1982 (2021).
[43]P. B. Allen and J. L. Feldman, "Thermal conductivity of disordered harmonic solids," Phys. Rev. B **48**, 12581–12588 (1993).
[44]Y. M. Beltukov, C. Fusco, D. A. Parshin, and A. Tanguy, "Boson peak and Ioffe-Regel criterion in amorphous siliconlike materials: The effect of bond directionality," Phys. Rev. E **93**, 023006 (2016).
[45]A. France-Lanord, E. Blandre, T. Albaret, S. Merabia, D. Lacroix, and K. Termentzidis, "Atomistic amorphous/crystalline interface modelling for superlattices and core/shell nanowires," J. Phys.: Condens. Matter **26**, 055011 (2014).
[46]K.-H. Lin and A. Strachan, "Thermal transport in SiGe superlattice thin films and nanowires: Effects of specimen and periodic lengths," Phys. Rev. B **87**, 115302 (2013).
[47]Y. Peng, J.U. Thiele, G. Ju, T. Nolan, Y. Ding, and A. Wu, "Recording layer for heat assisted magnetic recording," U.S. patent 8507114B2 (30 June 2011).
[48]A. Rajabpour, S. M. Vaez Allaei, Y. Chalopin, F. Kowsary, and S. Volz, "Tunable superlattice in-plane thermal conductivity based on asperity sharpness at interfaces: Beyond Ziman's model of specularity," J. Appl. Phys. **110**, 113529 (2011).
[49]M. Hu, J. V. Goicochea, B. Michel, and D. Poulikakos, "Thermal rectification at water/functionalized silica interfaces," Appl. Phys. Lett. **95**, 151903 (2009).
[50]G. C. Sosso, V. L. Deringer, S. R. Elliott, and G. Csányi, "Understanding the thermal properties of amorphous solids using machine-learning-based interatomic potentials," Mol. Simul. **44**, 866–880 (2018).
[51]B. Bhattarai, A. Pandey, and D. Drabold, "Evolution of amorphous carbon across densities: An inferential study," Carbon **131**, 168–174 (2018).
[52]T. Damart, V. M. Giordano, and A. Tanguy, "Nanocrystalline inclusions as a low-pass filter for thermal transport in a-Si," Phys. Rev. B **92**, 094201 (2015).
[53]M. Samanta, T. Ghosh, R. Arora, U. V. Waghmare, and K. Biswas, "Realization of both n- and p-Type GeTe thermoelectrics: Electronic structure modulation by $AgBiSe_2$ alloying," J. Am. Chem. Soc. **141**, 19505–19512 (2019).
[54]P. K. Schelling, S. R. Phillpot, and P. Keblinski, "Comparison of atomic-level simulation methods for computing thermal conductivity," Phys. Rev. B **65**, 144306 (2002).
[55]M. T. Dove, "Time correlation functions," in *Introduction to Lattice Dynamics*, Cambridge Topics in Mineral Physics and Chemistry (Cambridge University Press, 1993), pp. 229–232.
[56]A. Savitzky and M. J. Golay, "Smoothing and differentiation of data by simplified least squares procedures," Anal. Chem. **36**, 1627–1639 (1964).
[57]J. P. Boon and S. Yip, *Molecular Hydrodynamics* (Courier Corporation, 1991).
[58]P. Desmarchelier, A. Tanguy, and K. Termentzidis, "Thermal rectification in asymmetric two-phase nanowires," Phys. Rev. B **103**, 014202 (2021).
[59]Y. M. Beltukov, V. I. Kozub, and D. A. Parshin, "Ioffe-Regel criterion and diffusion of vibrations in random lattices," Phys. Rev. B **87**, 134203 (2013).

19 December 2023 12:28:58

Published under an exclusive license by AIP Publishing